

# Understanding as well as characterization of erratic interspike dynamics in semiconductor devices

Yuo-Hsien Shiau \*

Graduate Institute of Applied Physics, National Chengchi University, Taipei 11605, Taiwan, ROC

## ARTICLE INFO

### Article history:

Received 27 July 2010

Received in revised form

5 October 2010

Accepted 4 November 2010

by F. Peeters

Available online 11 November 2010

### Keywords:

A. Semiconductors

D. Interspike intervals

D. Ensemble Monte Carlo

D. Detrended fluctuation analysis

## ABSTRACT

The understanding of the origin of electronic noise would be very important in semiconductor devices. Detecting time characteristics via statistical approaches has been known to be useful in complex systems. In this study, the ensemble Monte Carlo particle method is used to simulate electron transport in a layered III–V semiconductor at room temperature. Nonlinear/erratic spiking fluctuations are predominant at the onset of current instabilities. To explore time characteristics detrended fluctuation analysis is used to analyze interspike intervals in different scales. Interestingly, multifractal behaviors are responsible for this kind of electronic noise. Therefore, it indicates that many extra time-characteristic would emerge in semiconductor devices, which would be strongly related to polar optical phonon scattering for intervalley transfer.

© 2010 Elsevier Ltd. All rights reserved.

## 1. Introduction

It is known that methods of statistical physics have been successfully applied to the study of spatial and temporal randomness in many disciplines, like the analysis of earthquake activities [1], neuronal firings [2–4], DNA nucleotide sequences [5], heartbeat time series [6–8], and security in encryption systems [9]. In particular, erratic interspike intervals (ISIs) appear very often in complex systems, which are the result of multiple time-scale dynamics, e.g., slow–fast dynamics. Recently, it is well accepted that fluctuations in complex systems carry important information reflecting the mechanisms underlying control processes and interactions among different components at multiple time scales. A major problem in the analysis of signals from complex systems is related to non-stationarities, e.g., mean and standard deviation vary with time. The presence of nonstationarities makes traditional approaches assuming stationary signals not reliable. To resolve the difficulties related to nonstationary behaviors, detrended fluctuation analysis (DFA) developed by Peng et al. [10,11] has been one of the powerful methods to detect self-similar scaling exponents embedded in a variety of natural systems.

In tradition, the small-signal response and noise spectral density have been used to analyze high-frequency fluctuations embedded in semiconductor devices. The actual tendency to reduce the dimensions of the active region of devices introduces

several complexities correlated to the presence of nonlinear effects in the applied voltage, e.g., hot-carrier effects. One of the typical examples is the study of spiking current fluctuations of GaAs structures below the onset of current instabilities, where the noise spectral densities at high frequencies show two resonant peaks associated with transit- and plasma-time effects. The resonant frequencies are respectively close to 20 GHz (transit frequency) and 1 THz (plasma frequency) [12]. Therefore, there are two characteristic time scales embedded in this device and slow–fast behaviors can be expected. However, it is known that the small-signal response function will be breakdown when the biased voltage is larger than the threshold for current instabilities. Besides, it can be expected that many extra time-characteristics would appear rather than the well-known transit- and plasma-time effects when applied voltages are near by and/or far from the threshold for current instabilities. Thus, it would be interesting to study spiking current fluctuations in semiconductor high-field transport by the use of different methods.

In this study, the ensemble Monte Carlo (EMC) particle method is used to simulate electron transport in a sandwiched structure under time-independent voltage bias  $U_{dc}$ . Different conduction modes (i.e., quenched/transit modes) are successfully generated from a lower bias to a higher bias. Particularly, irregular spiking fluctuations in the time domain are predominant in our EMC results. Based upon DFA results, we find that noisy ISIs exhibit multifractal behaviors, which indicate that multiple time scales are embedded in the present semiconductor device. Moreover, it can be believed that intervalley transfer from the  $\Gamma$ -valley to the  $L$ -valley as well as polar optical phonon scattering should be responsible for the present erratic fluctuations.

\* Tel.: +886 2 29393091; fax: +886 2 29360360.

E-mail address: [yhshiau@nccu.edu.tw](mailto:yhshiau@nccu.edu.tw).

The remainder of this paper is organized as follows. In Section 2, we briefly describe our approaches including EMC and DFA. Section 3 contains simulated electronic noise as well as DFA results. Discussions and concluding remarks are given in Sections 4 and 5, respectively.

## 2. Methods

**EMC approach:** One-dimensional EMC particle method is based upon the self-consistent solution of Poisson's equation and kinetic equations for one-electron distribution functions. A non-parabolic  $\Gamma$ ,  $L$ , and  $X$  three-band structure were taken into account in order to make the EMC model more realistic. Polar optical phonon scattering, acoustic phonon scattering, and ionized impurity scattering were incorporated. And the physical constants of GaAs were taken from Ref. [13]. In addition, the present EMC method adapts a simplified MEP (Maximum Entropy Principle) model [14] which can make the EMC simulation faster than the traditional calculations. As for the simulated geometry, the sandwiched semiconductor is denoted as  $n^+(0.8 \mu\text{m})-n^-(0.4 \mu\text{m})-n(4.0 \mu\text{m})-n^+(0.8 \mu\text{m})$ , and the doping concentration in  $n^+$ ,  $n^-$ , and  $n$  regions are, respectively, equal to  $100.0 \times 10^{15} \text{ cm}^{-3}$ ,  $0.2 \times 10^{15} \text{ cm}^{-3}$ , and  $5.0 \times 10^{15} \text{ cm}^{-3}$ . The highly doped  $n^+$  layer close to the doping notch  $n^-$  is connected to cathode and the other  $n^+$  layer is connected with anode. Thus, there is no potential drop in both  $n^+$  layers and the function of the  $n^-$  layer is for the hot-electron injector. To increase  $U_{dc}$  from low to high values, quenched as well as transit conduction modes can be numerically observed via the measurement of space–time evolution of the electric field, from which ISIs can be obtained for further analysis.

**DFA approach:** The time series  $x(i)$  to be analyzed is first integrated and denoted as  $y(i)$ , where  $i = 1, \dots, N$  and  $N$  is the length of the series. Next, the integrated time series is divided into boxes of equal length,  $s$ . In each box of length  $s$ , a least squares line (or polynomial curves) is fitted to the data to represent the trend in that box. Next, the integrated time series is detrended by subtracting the local trend in each box. The root-mean-square (RMS) fluctuation of this integrated and detrended time series is calculated and denoted as the 1st order fluctuation function  $F(s)$ . This computation is repeated over all box sizes to characterize the relationship between  $F(s)$  and  $s$ . Typically,  $F(s)$  will increase with the box size  $s$ . A linear relationship in a log–log plot indicates the presence of a monofractal spectrum:

$$F(s) \propto s^\gamma. \quad (1)$$

It would be helpful to understand the statistical meaning of the exponent  $\gamma$  through the following explanations. For stationary data with scale-invariant temporal organization, the Fourier power spectrum is proportional to  $f^{-\beta}$ , where the scaling exponent  $\beta$  is related to  $\gamma$  with that way,  $\beta = 2\gamma - 1$ . Thus time series with the  $1/f$  characteristic (i.e.,  $\beta = 1$ ), sometimes named positive correlations, is characterized by exponent  $\gamma$  being equal to 1. As for Gaussian white noise of the flat band,  $\beta = 0$  and, therefore,  $\gamma = 0.5$ . When  $\beta$  is smaller than 0, i.e.,  $\gamma \leq 0.5$ , it indicates that negative correlations are predominant in the original data. In general, it is not always possible to exhibit a monofractal scaling for analyzed data, and exponent  $\gamma$  could be different in different box size  $s$ .

## 3. Results

Four panels in Fig. 1 illustrate different transport modes when  $U_{dc}$  is increased from a lower bias (1.2 V) to a higher bias (1.8 V), where the  $x$  symbol represents space and the horizontal axis is time. Panel I is a time-independent case, in which the applied voltage is below the threshold for spontaneous current oscillations.

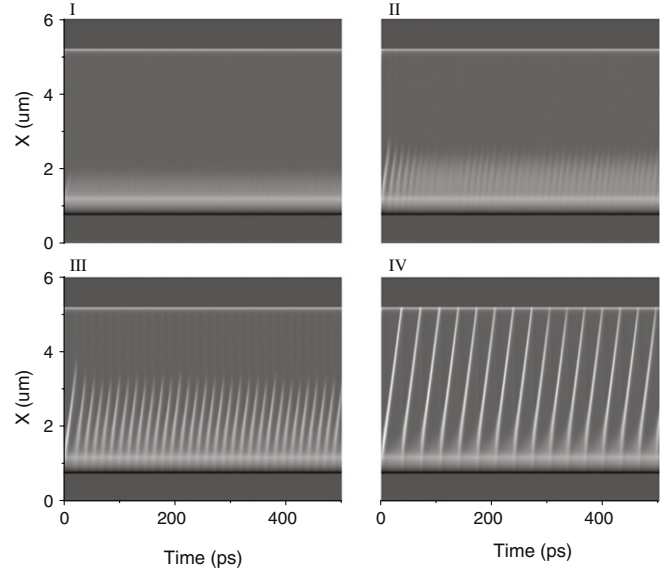


**Fig. 1.** Space–time evolution of the electric field for  $U_{dc} = 1.2$  V (panel I), 1.5 V (panel II), 1.65 V (panel III), and 1.8 V (panel IV), where the bright area corresponds to the high-field regime.

Erratic quenched modes, i.e., irregular annihilation of the high-field profile before reaching to the anode, are illustrated in panels II and III, and the appearance of periodic transit modes is shown in panel IV. It would be easy to check that the applied field located in both  $n^-$  and  $n$  regions from panels I–IV is, respectively, equal to 2.75 kV/cm, 3.41 kV/cm, 3.75 kV/cm, and 4.54 kV/cm. Therefore, panels III and IV are operated at the regime of negative differential mobility (NDM), where the threshold field for GaAs is around 3.50 kV/cm. It should be noted that the average traveling distance for quenched dynamics will be increased via the increment of the applied voltage. And the propagating velocity  $v$  for the high-field profile will be decreased to a saturated value when  $U_{dc}$  is increased to near 17.6 V. According to numerical results, it is found that the average transport periodicity in panel III is around 15 ps, but in panel IV periodicity will be increased to near 33 ps. Therefore, transit frequencies in panels III and IV are, respectively, corresponding to 66.7 GHz and 30.3 GHz. Concerning on the topic of ISIs shown in the present system, it may define annihilation–position sequences of the high-field profile as ISIs, i.e.,  $x(1), x(2), \dots, x(N-1), x(N)$ . Furthermore,  $x(i)/v$  is associated with time intervals of spiking current fluctuations.

In order to analyze electronic noise shown in the lower panel of Fig. 2, we take the difference between two successive annihilated positions (named position return, PR) from ISIs, and treat PR data as a new-generated time series which is illustrated in the upper panel of Fig. 2. The absolute value of PR divided by the propagating velocity of high-field profiles is characterized as transit-time variability (TTV). If periodic quenched (or transit) modes exist, PR should be equal to zero and there is no TTV. In Fig. 2 it is obvious to see that PR exhibits a complicated manner, and Fig. 3 illustrates DFA results for PR data. The nonlinear curve shown in Fig. 3 indicates that multiple time scales are embedded in the present quenched dynamics, where the time scale is defined as the box size  $s$  multiplied by the average transport periodicity. In particular, the scaling crossover can be observed at  $\log_{10} s \approx 0.9$ . In the short-term fluctuations ( $0 < \log_{10} s \leq 0.90$ ),  $\gamma$  is approximately equal to 0.30. Concerning the long-term fluctuations ( $\log_{10} s \geq 0.90$ ),  $\gamma$  will be significantly decreased to near 0.05. It is believed that in the mathematical point of view the scaling crossover is resulted from the competition between two different signals [15], and each of the signals has its own scaling characteristics. Owing to that,

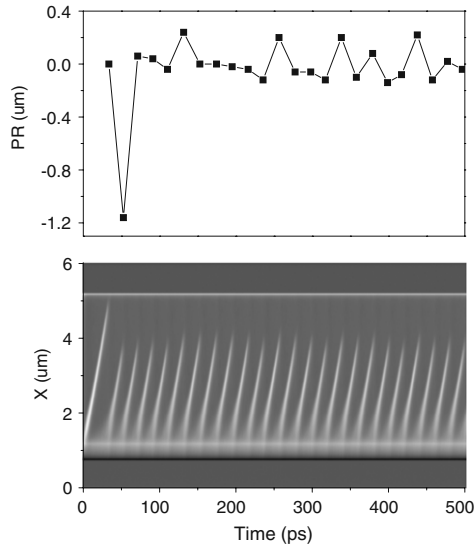


**Fig. 2.** Lower panel: Space–time evolution for  $U_{dc} = 1.74$  V. Compared to the panel III of Fig. 1, the traveling distance of high-field profiles will become longer. Upper panel: The schematic illustration of fluctuating PR data obtained from the result of lower panel. It shall be noted that we take PR data for further analyses when  $t$  is larger than 100 ps.

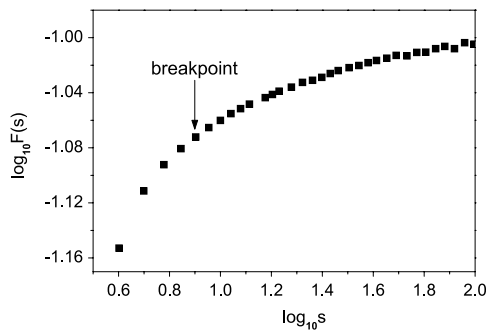


**Fig. 3.** DFA results for fluctuating PR data when  $U_{dc} = 1.74$  V. The breakpoint is used to differentiate short- and long-term fluctuations.

multifractal behaviors in this study are numerically observed in erratic transport fluctuations.

It shall be noted that the plasma frequency in our study can be realized through the quantity named the mean value of TTV, which is approximatively equal to 0.2 ps in Fig. 2 and its corresponding frequency is 5 THz. In physics it is known that the doping concentration in  $n^+$ -regions will determine the plasma frequency which is independent of applied voltage [12]. In panels II and III of Fig. 1 we also find that the mean value of TTV is close to 0.2 ps, thus the plasma frequency can be realized in erratic transport fluctuations.

#### 4. Discussions

It is well known that NDM observed in GaAs is due to intervalley transfer between the lower and upper valleys, the  $L$  (upper) valley electrons being heavier, and thus slower, than electrons in the  $\Gamma$  (lower) valley. Moreover, polar optical phonon scattering has been believed to be a dominant energy loss mechanism for intervalley transfer. It can be analytically proved that beyond 2.42 kV/cm the power gained from the applied field exceeds that lost due to polar optical phonon scattering, which leads to dramatical increase in the electron energy and is responsible for the onset of intervalley transitions [16]. In this study, cyclic transport can be observed in panels II and IV of Fig. 1, but time-independent

conduction mode will show up when the applied field is smaller or slightly larger than 2.42 kV/cm (panel I). In particular, erratic quenched conduction in panels II and III indicates that intervalley transfer in GaAs is a nonstationary dynamical process, but that phenomenon will disappear when the applied field is much larger than 2.42 kV/cm (panel IV). The main reason we think is that the number of electrons to participate in intervalley transitions could be nonstationary at intermediate fields, thus it influences the formation time of high-field profiles from the doping notch (i.e.,  $n^-$ -region) which is usually used as the hot-electron injector [17].

The classical drift–diffusion theory is known to well describe transport phenomena in systems with a larger size, which should be much larger than the mean free path for elastic (impurity) scattering as well as the phase-relaxation length for inelastic (phonon or electron–electron) scattering. Therefore, momentum and energy relaxations occur faster than all other processes, which can be eliminated adiabatically in hydrodynamic balance equations. In our previous results under the classical drift–diffusion model periodic quenched modes can be numerically observed in a larger  $n^+$  (8.0  $\mu\text{m}$ )– $n^-$  (4.0  $\mu\text{m}$ )– $n$  (40.0  $\mu\text{m}$ )– $n^+$  (8.0  $\mu\text{m}$ ) device [17]. However, in the present study the EMC approach is used to simulate the Boltzmann transport equation, in which all scattering processes such as phonon, impurity, and electron–electron scattering are included. Owing to this, we may reasonably conclude that many extra time-characteristics shown in Fig. 3 would be from scattering processes, in particular, the primary factor would be polar optical phonon scattering which determines the number of electrons to participate in intervalley transitions. Thus the DFA plot shown in Fig. 3 is mainly responsible for the non-stationary polar optical phonon scattering. The signature of other scattering processes embedded in the DFA plot would be hard to isolate because dominant RMS fluctuations are from polar optical phonon scattering. Therefore, the present study offers a way to characterize the nonstationary scattering process, which might be complementary to the results reported by O’Leary et al. [16].

#### 5. Conclusions

In conclusion, we study nonlinear transport phenomena in a GaAs-based sandwiched semiconductor at room temperature by using the EMC particle method. Transit and plasma frequencies can be directly computed via transport processes rather than noise spectral density. Moreover, DFA results suggest that multiple time scales are embedded in the present system operated at the onset of current instabilities. It can be believed that the nonstationary processes observed in electron transport would be strongly related to polar optical phonon scattering for intervalley transfer. Therefore, fractal analysis provides a different point of view on electron noise in semiconductor devices.

#### Acknowledgement

This work was supported by the National Science Council of the Republic of China (Taiwan) under Contract Nos. NSC 95-2112-M-259-010-MY3.

#### References

- [1] L. Telesca, V. Lapenna, M. Macchiato, *Physica A* 354 (2005) 629.
- [2] S. Blesić, S. Milošević, Dj. Stratimirović, M. Ljubisavljević, *Physica A* 268 (1999) 275.
- [3] S. Blesić, S. Milošević, Dj. Stratimirović, M. Ljubisavljević, *Physica A* 330 (2003) 391.
- [4] K. Robin, N. Maurice, B. Degos, J.-M. Deniau, J. Martinerie, L. Pezard, J. Neurosci. Methods 179 (2009) 142.
- [5] S.V. Buldyrev, N.V. Dokholyan, A.L. Goldberger, S. Havlin, C.-K. Peng, H.E. Stanley, G.M. Viswanathan, *Physica A* 249 (1998) 430.
- [6] S. Havlin, L.A.N. Amaral, Y. Ashkenazy, A.L. Goldberger, P.Ch. Ivanov, C.-K. Peng, H.E. Stanley, *Physica A* 274 (1999) 99.

- [7] Y.-H. Shiau, *Auton. Neurosci. Basic Clin.* 146 (2009) 62.
- [8] Y.-H. Shiau, *Auton. Neurosci. Basic Clin.* 152 (2010) 119.
- [9] Y.-H. Shiau, M.-C. Wu, *Opt. Commun.* 283 (2010) 1909.
- [10] C.-K. Peng, S.V. Buldyrev, S. Havlin, M. Simons, H.E. Stanley, A.L. Goldberger, *Phys. Rev. E* 49 (1994) 1685.
- [11] C.-K. Peng, S. Havlin, H.E. Stanley, A.L. Goldberger, *Chaos* 5 (1995) 82.
- [12] L. Reggiani, P. Golinelli, L. Varani, T. González, D. Pardo, E. Starikov, P. Shiktorov, V. Gružinskis, *Microelectron. J.* 28 (1997) 183.
- [13] K. Brennan, K. Hess, *Solid-State Electron.* 27 (1984) 347.
- [14] V. Romano, *J. Comput. Phys.* 176 (2002) 70.
- [15] K. Hu, P. Ivanov, Z. Chen, P. Carpena, H. Stenely, *Phys. Rev. E* 64 (2001) 011114.
- [16] S.K. O'Leary, B.E. Foutz, M.S. Shur, L.F. Eastman, *Solid State Commun.* 118 (2001) 79.
- [17] Y.-H. Shiau, *J. Phys. Soc. Japan* 78 (2009) 115001;  
Y.-H. Shiau, *Solid State Commun.* 139 (2006) 278;  
Y.-H. Shiau, Y.-F. Peng, *Solid State Commun.* 139 (2006) 114;  
Y.-H. Shiau, *Solid-State Electron.* 50 (2006) 191;  
Y.-H. Shiau, Y.-F. Peng, *Phys. Rev. E* 71 (2005) 066216.